Soft Matter

PAPER

On the measurement of the surface pressure in Langmuir films with finite shear elasticity

Elodie Aumaitre,[a] Dominic Vella†[b] and Pietro Cicuta*[a]

We investigate the use of the Wilhelmy plate method to measure the surface pressure in a solid-like Langmuir film under compression. Layers of the protein hydrophobin, which exhibits a high shear elastic modulus, are spread and compressed in a Langmuir trough. The resulting isotherms are classified according to the surface pressure and distance between the barriers measured at the onset of buckling. We find that the surface pressure measured in the centre of the layer at the onset of buckling decays with increasing distance between the barriers (which can be tuned by varying the amount of material spread initially). However, unlike the case of particle rafts, the length scale of this decay is not controlled by the width of the trough but rather by the size of the Wilhelmy plate used. We use experiments and a computational model to suggest that this independence of trough width may be attributed to the localised nature of the effect of the trough walls. Our work highlights the potential pitfalls of using the Wilhelmy method to characterize layers with high shear rigidity and may lead to a better understanding of the use of the Wilhelmy plate to measure the surface stress tensor.

1. Introduction

Since its development by Wilhelmy in 1863,[1] the measurement of the vertical force exerted on a partially submerged and wetted plate has become ubiquitous as a straightforward and inexpensive method for measuring the tension of liquid–fluid interfaces.[2] The Wilhelmy plate has also been successfully employed to determine the surface dilatational modulus for a range of proteins and polymers by monitoring surface pressure variations in a Langmuir trough.[3] Dilatational elasticity is the primary factor affecting the stability of emulsions and foams.[4,5] Over the years, the accuracy and even the validity of this technique have been challenged on various grounds. Sources of error inherent to the method itself can arise from incomplete wetting of the plate, the effect of the edges of the plate[6] and additional surface area created by the presence of a dipped plate in a Langmuir trough.[7] By and large, however, these issues can be controlled, and the Wilhelmy plate gives reliable measurements of the tension of liquid–air and liquid–liquid interfaces.

The validity of the Wilhelmy plate technique when probing the surface tension of rigid films remains a much more open question, and is the subject of the present work. For example, the orientation of the plate has been found to be an important factor when the layer develops a shear modulus during compression.[8,9] In this case the surface pressure should be considered to be a tensorial quantity; the difference between the surface pressures measured by plates placed parallel and perpendicular to the compressing barriers can be used to measure the shear modulus. Other studies have questioned the interpretation of the values measured. Cicuta and Vella[10] showed that, for particle rafts, the pressure measured in the centre of the trough at the moment of buckling decays exponentially with the trough aspect ratio. Since buckling is believed to occur only when the surface pressure reaches the value of the surface tension of the clean interface, they inferred that this exponential decay corresponds to a decaying stress profile within the raft. They rationalised this inhomogeneous stress profile as being a result of friction from the trough walls. It is natural then to wonder whether similar effects lie hidden in the data obtained with other rigid or elastic Langmuir films. Indeed, the literature offers many examples where the isotherms recorded during compression of layers in a Langmuir trough display unexpected behaviour. Surface pressure gradients along the compression axis have been reported previously by Peng and Barnes for polyvinyl stereate monolayers[11] and by Mate *et al.* in silica particle layers.[12] The latter hypothesized that the cohesiveness of the particulate layer may be the origin of the pressure gradient. Prins and van Kalsbeek[13] have also suggested that friction at the trough walls might reduce the measured surface pressure for monolayers with shear properties.

The Wilhelmy plate itself may also perturb the stress field in an elastic layer. Kumaki *et al.*[14] and Yim *et al.*[15] studied particulate

[a] Cavendish Laboratory, University of Cambridge, JJ Thomson Avenue, CB3 0HE Cambridge, UK. E-mail: pc245@cam.ac.uk
[b] ITG, Department of Applied Mathematics and Theoretical Physics, University of Cambridge, Wilberforce Road, Cambridge, CB3 0WA, UK
† Present address: OCCAM, Mathematical Institute, 24-29 St Giles', Oxford, OX1 3LB, UK

monolayers composed of polystyrene and polyimide particles, respectively. These 'Brownian particle rafts' display a significant shear modulus and both studies found that the surface pressure measured by means of a Wilhelmy plate is considerably lower than that measured by a floating barrier. More recently Witten et al.[16] showed theoretically that, for the case of a circular plate in a circular trough, the radial stress will vary strongly in the radial direction being maximum at the plate.

The present work attempts to understand the variability of the surface pressure recorded in rigid layers. To do so, it is useful to monitor a particular event that occurs at a fixed reference surface pressure. For protein films, collapse can take several forms and has been frequently discussed in the literature.[17] The formation of out-of-plane wrinkles (buckling) is one common collapse phenomenon and is believed to occur when the interfacial tension reaches zero. Theoretical[18] and computational[19] studies agree that the film buckles when its surface pressure reaches the surface tension of the pure subphase, i.e. at zero interfacial tension. The onset of buckling is therefore a natural reference point, and the one chosen for this study. The fact that experimental data do not always confirm this prediction, and that buckling surface pressures are sometimes observed to be lower than the surface tension of the subphase,[20] should be borne in mind. We will reconsider this in light of the results presented here.

The protein hydrophobin serves as an excellent model for investigating the effect of a large shear rigidity. Hydrophobin films have a large shear elastic modulus, and out of plane buckling occurs during compression leading to wrinkles that are visible to the naked eye. The Class II hydrophobin (HFBII) is derived from the filamentous fungus Trichoderma Reesei. Its ability to form a very elastic and shear resistant film offers great potential for applications ranging from foam stabilisation to surface modification agents for biomedical devices.[21] Remarkably high values of the surface elastic and shear moduli have been reported for layers of hydrophobin HFBII.[22,23] Surface pressure isotherms have already been recorded using a Wilhelmy plate for hydrophobin films compressed in a Langmuir trough. These isotherms show a smooth rise followed by a sharp slope discontinuity corresponding to the collapse of the monolayer by wrinkling.[23,24] Another characteristic of hydrophobin layers is that the surface pressure isotherm exhibits large hysteresis on re-expansion, along with a shift to smaller areas upon repeated compression-expansion cycles. These effects are thought to result from the re-arrangement of the molecules into more compact layers following each cycle.

In this article, we study the effect of trough and plate geometry on the surface pressure measured at buckling for hydrophobin films. Our experimental data reveal that the surface pressure at the onset of buckling decays as the distance between the barriers at buckling increases. Furthermore, the length scale of this decay is proportional to the plate width. In contrast to what was observed for granular particle rafts by Cicuta and Vella,[10] the width of the trough does not appear to affect the surface pressure measured at buckling, provided that the width is greater than some critical value whose value we discuss. This observation is consistent with visualization of the strain pattern within the surface layer, which shows that the friction of the walls strongly affects the strain field in the vicinity of the walls, but the deformation rapidly decays away from the walls.

2. Materials and methods

2.1. Hydrophobin

Class II hydrophobin (HFBII) from Trichoderma Reesei was a gift from Unilever Global Development Centre and was obtained from VTT Biotechnology (Espoo, Finland). Details of the preparation are described elsewhere.[25,26] The stock solution has a concentration of 7.1 mg ml^{-1} and was stored frozen. The sample can be stored in the fridge during experiments and can sustain multiple thawing/freezing cycles without degrading. Before each experiment, the hydrophobin sample was sonicated for one minute.

2.2. Langmuir trough

Multiple droplets, each of volume 1 μL, are deposited gently (using a microsyringe) onto a subphase consisting of de-ionised water (ElgaStat UHQII, Elga Process Water, resitivity of 18 MΩcm) contained within a Langmuir trough. This process leads to the formation of a layer consisting of a total amount spread in the range 12 μg to 110 μg. The Langmuir trough is a model 611 (Nima Technology, Coventry, UK), with maximum dimensions: length $L = 30$ cm and width $w = 20$cm. The sample was spread with the barriers fully opened. The layer is then allowed to equilibrate for 20 min after spreading before compression is started. The temperature of the subphase was set to 22 °C and maintained by a cooling bath (BC20, Fisher Scientific). Two computer-controlled barriers allow the symmetrical compression of the layer at a constant speed in the range 10–100 cm^2 min^{-1}. Unless stated otherwise, the data in this paper is obtained from compressions at 30 cm^2 min^{-1}. The trough was cleaned thoroughly and a fresh protein layer spread for each run of the experiment because hydrophobin layers undergo irreversible changes after just one compression.

Based on the observation by Cicuta and Vella[10] that the width of the trough may play an important role for particle rafts, it was thought that this may also be an important feature in the present system. To test this possibility, the width of the trough was varied by placing custom-made strips of Perspex perpendicular to the trough barriers (Fig. 1), in such a way that the surface layer is confined to the middle section of the trough. In this study, five
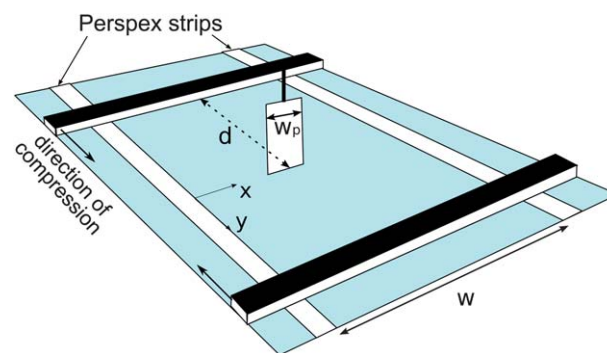

Fig. 1 Diagram of the Langmuir trough setup showing placement of Wilhelmy plate and dimensions. Perspex strips are placed in the trough to modify the trough width w. d corresponds to the barrier to sensor distance and w_p to the width of the plate.

different effective trough widths were studied by varying the distance between the strips: w = 20,15,10,5 and 3 cm. The possible effect of a meniscus was limited by ensuring that the trough was filled to be flush with the top surface of each strip.

2.3. Surface pressure measurement

The surface pressure of a layer is defined to be $\Pi = \gamma_c - \gamma_{layer}$, where γ_c is the surface tension of the clean air–water interface (γ_c = 72 mN m^{-1}) and γ_{layer} is the surface tension of the interface covered with protein. The surface pressure is measured using a Wilhelmy plate hung from a microbalance sensor (type PS4, Nima Technology). Wilhelmy plates made of filter paper or platinum were used, though the plate material does not seem to affect the results obtained. The Wilhelmy plate was placed in the centre of the trough and kept in a vertical position and parallel to the barriers thanks to a specially designed rigid hook. The plate provides reliable measurements only when placed midway between the two barriers; when placed off-axis, asymmetric forces exerted on the plate result in its horizontal displacement, and hence to erroneous measurements. To investigate the effect of the plate width on the surface pressure measured, four Wilhelmy plates of different widths were used: w_p = 0.25 cm, 0.5 cm, 1 cm and 2 cm.

2.4. Analysis of isotherms

The Class II hydrophobin HFBII protein exhibits a high shear modulus and collapses by out-of-plane buckling.[22] The onset of buckling can be determined from the 'rolling off' in the surface pressure isotherm, which corresponds to the appearance of wrinkles to the naked eye. To automate the detection of this point we note that the 'rolling off' of the isotherm corresponds to the maximum in the curvature of the isotherm and so can be found as the minimum of the second derivative of the surface pressure isotherm, viewed as a function of area (Fig. 2). To obtain buckling at a range of plate-barrier distances, the amount of hydrophobin spread was varied and a surface pressure compression isotherm recorded for each amount. As expected, there is a linear correlation between the amount of hydrophobin spread and the distance between the barriers at the onset of buckling. Fig. 3 shows that the molecular area at buckling remains reasonably constant as the barrier-to-sensor distance at buckling varies. The mean value is around 347 $\mathring{A}^2$ with a standard deviation of 84 $\mathring{A}^2$. The largest source of error in this measurement is the variation in the amount of hydrophobin spread. Such errors can originate from errors in the volume spread or bad spreading, which may lead to the sinking of some of the hydrophobin molecules into the subphase. From this graph, we conclude that buckling occurs at a constant area per molecule regardless of the geometric area occupied by the layer. This confirms that buckling is a physical property of the layer and can be used as a reference point to characterise hydrophobin isotherms.

2.5. Analysis of strain field

Though it is difficult to measure the state of stress within the layer, it is easier to measure the state of strain, as was shown by Malcolm[27] using sulfur lines spread onto the layer at low surface
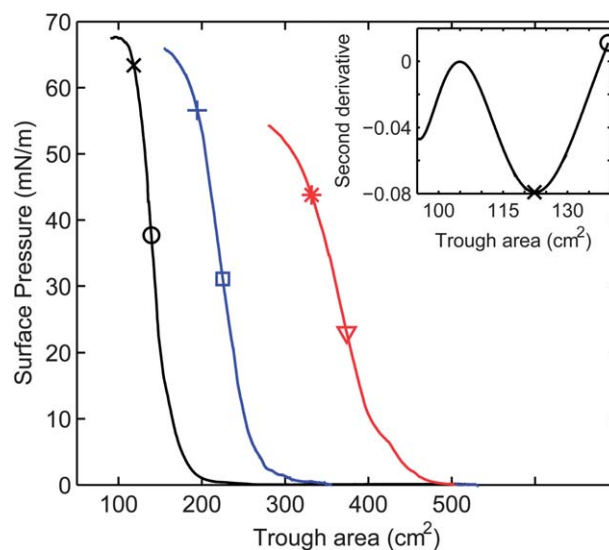

Fig. 2 The isotherms of compression depend on the different amounts of hydrophobin spread. From left to right: 36 μg, 58 μg and 85 μg. The open markers indicate the inflexion point while the points mark the onset of buckling. The surface pressure and trough area at buckling (Π_{buck}, Area$_{buck}$) are recorded for each isotherm. The inset figure displays the second derivative of the isotherm as a function of area for areas smaller than the inflexion point. Here 36 μg of hydrophobin has been spread. The local minimum corresponds to the onset of buckling.
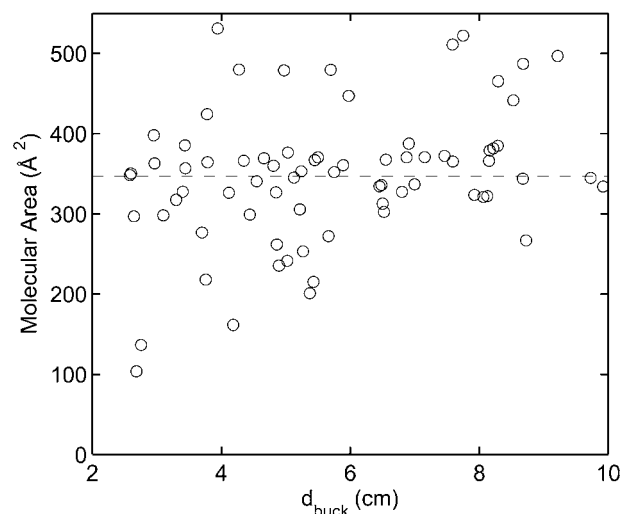

Fig. 3 Buckling happens at a well defined molecular area. The data shows the molecular area at buckling, *versus* the barrier-to-sensor distance at buckling, obtained from isotherms with different spread amounts. The dashed line represents the average value of 347 $\mathring{A}^2$. The standard deviation is 84 $\mathring{A}^2$.

pressure. We therefore sprinkled a series of sulfur lines through a custom-made mask onto the protein layer when Π = 10 mN m^{-1}. At this surface pressure the layer has sufficient rigidity to support the sulfur powder. With further compression, the sulfur powder lines track the displacement of the layer, and are visibly distorted, providing a direct representation of the spatial structure of the strain field within the layer. Movies are recorded at a frame rate of 15 frames per second during compression. We

use an AVT Pike CCD Camera mounted with an AF Micro-Nikkor 60 mm f/2.8D objective.

3. Results and discussion

Fig. 2 shows surface pressure isotherms for three different amounts of hydrophobin spread at the interface. For layers having a negligible shear elasticity such as the liquid phases of lipids,[2,28,29] polymers such as PVAc[30] and various proteins[3,31] it is well known that area-pressure isotherms obtained with different spread amounts can be overlaid with one other by using the area per molecule as abscissa. It is clear from Fig. 2 that the hydrophobin isotherms differ dramatically with the spread amounts. Indeed, the surface pressure at buckling decreases as the distance between the barriers at buckling increases, as shown in Fig. 4. An

Fig. 4 The surface pressure at bucking depends on the distance to the barriers at bucking, and on the width of the plate. (a) Surface pressure at the onset of buckling Π_{buck} versus the distance between the sensor and the barrier d_{buck} for *trough widths* of 3 cm ($\blacktriangledown$), 5 cm ($\blacktriangle$), 10 cm ($\bullet$), 15 cm ($\blacksquare$) and 20 cm ($\blacklozenge$). Solid lines are fits to a linear function $\Pi_{buck} = \Pi_0(1 - x/L)$, where $(\Pi_0, L) = (58, 13)$ for a 3 cm wide trough but the data for trough widths of 5 to 20 cm fall onto the same linear decay, $(\Pi_0, L) = (61, 44)$. Here the plate width is $w_p = 1$ cm. (b) Comparison of the surface pressure Π_{buck} versus the distance between the sensor and the barrier d_{buck} at the onset of buckling for *plate widths* $w_p = 0.25$ cm ($\square$), 0.5 cm ($\triangle$), 1 cm ($\diamond$) and 2 cm ($\circ$). Each set of data are fitted by a linear regression $\Pi_{buck} = \Pi_0(1 - x/L)$ where $(\Pi_0, L) = (77, 13)$, $(74, 20)$, $(61, 44)$, $(57, 80)$ for plate widths of 0.25 cm, 0.5 cm, 1 cm and 2 cm respectively. Π_0 values are in mN m^{-1} and L values are in cm; the precision in the fitted parameters reported here is ± 0.5 for Π_0 and ± 2 for L.

analogous phenomenon was recently observed in particle rafts,[10] and attributed to friction with the trough walls. In the case of particle rafts, it was found that the width of the trough controlled the decay in surface pressure at buckling. Fig. 4a shows the surface pressure at buckling as a function of the distance between the two barriers for different values of the trough width. We observe that for all but the narrowest trough width ($w = 3$ cm) the decay in surface pressure at buckling appears to be independent of trough width.

Fitting the surface pressure at buckling to a linear relationship

$$\Pi_{buck} = \Pi_0(1 - d_{buck}/L)$$

we obtain a characteristic length scale L for the decay. We note that the data appear to be well fitted by a linear relationship but that they could also be fitted with an exponential law in which the distances d_{buck} presented here are small compared to the length scale of the exponential decay. Dimensional analysis shows that this length scale must be set by some length within the system and so, with the trough width already excluded, we turn to the width of the Wilhelmy plate. Fig. 4b shows experimental data obtained by using Wilhelmy plates of different widths. These results show a strong dependence of the surface pressure at buckling on the plate size. Fig. 5 shows that the length scale of the decay, L, grows linearly with the plate width. For the smallest plate ($w_p = 0.25$ cm) the surface pressure at buckling shows a very strong sensitivity to the distance between barriers. However, with the largest plate ($w_p = 2$ cm) we observe a much smaller sensitivity to the distance between the two barriers at buckling (Fig. 4b). We emphasize that the difference in surface pressure recorded by each plate is large enough that it cannot be attributed to experimental errors linked to the use of a Wilhelmy plate. Common experimental complications (*e.g.* loss of material on the plate, extra surface area due to the plate, and edge effects) would be expected to lead to variations of pressure of less than 1 mN m^{-1},[32] much smaller than the effect observed here. We also note that the effect reported here cannot be attributed to changes in the contact angle (through hydrophobization of the plate) since an increase in the contact angle would reduce the surface tension force on the plate leading to an anomalously large apparent surface pressure (rather than the decrease in surface pressure measured here). In Appendix 1 a control experiment is described that excludes dynamical relaxation as the cause of the results in Fig. 4.

Fig. 3, which shows that the molecular area is constant with the barrier-to-sensor distance at buckling, confirms that buckling is a physical property of the layer and that the variability in the surface pressure measured at buckling is a characteristic of the Wilhelmy plate measurements. Kisko et al.[33] reported a value of 21 Å for the diameter of an hydrophobin HFBII monomer, leading to an area of 346 Å^2 occupied by each molecule of hydrophobin. We found a mean value for the molecular area at buckling of 347 Å^2, showing that buckling occurs when the hydrophobin molecules, which behave essentially as hard spheres, cannot be compressed any further.

As discussed before, buckling has been reported to occur at surface pressures lower than the corresponding surface tension of the subphase in some systems. We note here that measuring the surface pressure at buckling using a Wilhelmy plate can lead to
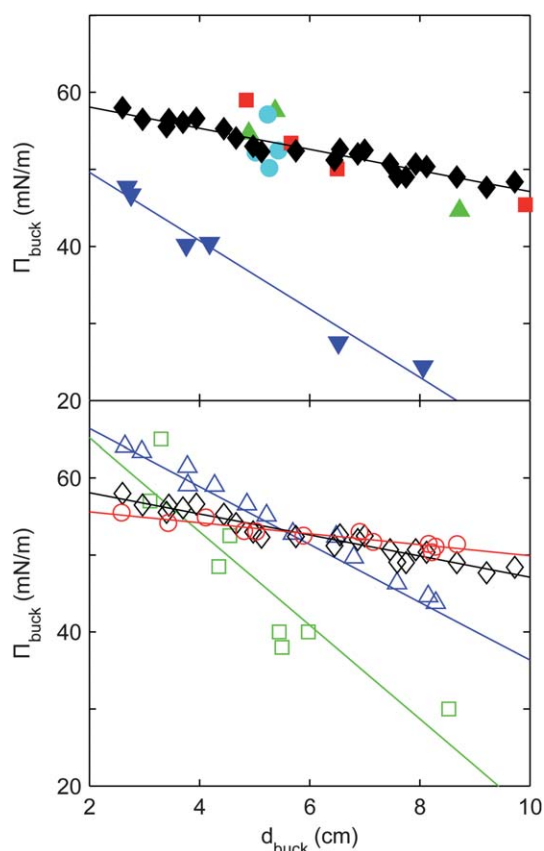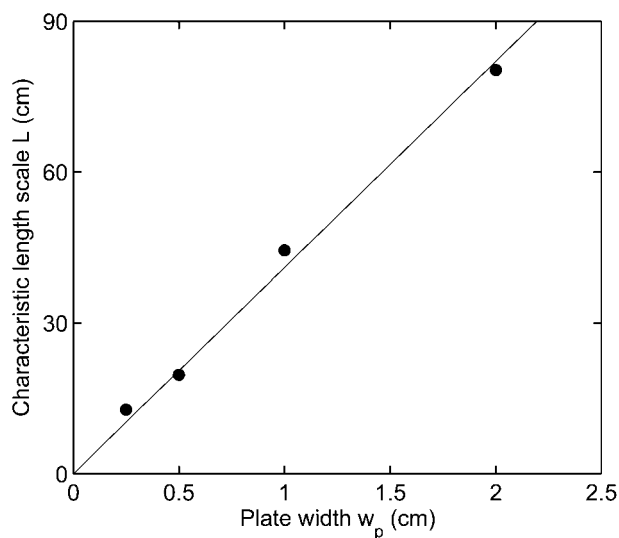
Fig. 5 The length scale of the surface pressure decay with the barrier-to-sensor distance is proportional to the plate width. These data, corresponding to the four datasets in Fig. 4b, are interpolated by a linear regression $L = 41 \times w_p$.

Fig. 6 The strain field can be measured, and described theoretically. Snapshots show sulfur lines sprinkled on a hydrophobin layer before compression (a), and after compression (b) and (c). Approximately one quarter of the trough is imaged. The initial position of the lines is indicated by dashed horizontal lines in each case. The solid curves in (b) and (c) show the theoretically determined shape of these lines after compression, as determined from the calculation outlined in Appendix 2. Here we take Poisson ratio $\nu = 0.5$ and two different values of the wall friction coefficient μ: in (b) $\mu = 0.5$ and in (c) $\mu = 0.75$.

friction. Furthermore, the numerical results show that the effect of the wall is felt over roughly half of the trough's half-width. We conclude from this that if the Wilhelmy plate is wide enough that it penetrates the region affected by the presence of the wall then the surface pressure measurements may also be affected by the presence of the wall. For the experiments presented here only those with $w = 3$ cm and $w_p = 1$ cm (▼) in Fig. 4a satisfy this criterion. We therefore believe that the wall friction is likely to be responsible for the reduced surface pressure found experimentally when the trough width is decreased to $w = 3$ cm.

4. Conclusion

We have shown experimentally that the measurement of the surface pressure of a rigid film using a Wilhelmy plate is complicated by at least two factors that have not been found to be important in fluid layers: the friction from the sides of the trough and the effect of the plate itself, acting as an inclusion in the layer. We have observed that the geometry of the setup affects the compression isotherms in two important ways. Firstly, the buckling pressure that is measured at the onset of buckling decreases with increasing distance between the barrier and sensor at buckling. The collapse pressure that is measured, and more generally the entire isotherm will therefore depend on the amount of protein spread at the interface in a way that cannot simply be rescaled by using area per molecule as independent variable. Secondly, the sensitivity of the collapse pressure to the distance between the barriers at collapse depends on the width of the plate itself: the length scale of the decay observed is proportional to the plate width. This is similar to the qualitative results of Witten et al.[16] who suggested that the radius of a cylindrical Wilhelmy plate in a circular Langmuir trough would influence the surface pressure measurement. However, this is the first experimental demonstration of such an effect and is significantly different to that predicted by the analysis of Witten et al.[16] We believe that such a difference is likely to be due to the geometry difference between the idealised situation considered theoretically[16] and the standard experimental setup used here.

a lower value than expected, see Fig. 4, in the presence of shear elasticity.

We see that, generally speaking, the width of the trough has very little influence on the surface pressure measured at buckling. Rather, the surface pressure measured at buckling is controlled by the width of the Wilhelmy plate in some manner that is not yet understood. However, we also see that results obtained with the narrowest trough, $w = 3$ cm, do show a different behaviour to that observed with wider troughs. It is natural to wonder if this difference may be attributed to the effect of friction induced by the trough walls on the layer. A cohesive film might be able to sustain the friction forces generated by the walls and hence reduce the effective surface pressure measured in the centre of the trough. To investigate this possibility, a probe of the strain field is achieved by observing the deformation due to compression of material lines that are initially horizontal. These material lines are visualized by sprinkling sulfur powder onto the hydrophobin monolayer. The deformation of these lines is shown in Fig. 6, and a theoretical model describing the strain field is outlined in Appendix 2.

The most remarkable feature of the deformed lines is that the perturbation of their shape near the wall appears to be localised close to the wall. A more detailed phenomenological study of the sulfur lines deformation can be found in Appendix 3. To test whether this observation is consistent with the effect of wall friction we use a mathematical model described in detail in Appendix 2. This mathematical model treats the layer as an elastic sheet in compression, with wall friction parametrized by a friction coefficient μ. The model allows us to calculate the predicted position of the original lines after compression and compare the result to that observed experimentally. Such a comparison is shown in Fig. 6 for two different values of μ. This comparison shows good agreement between the model predictions and experiment suggesting that the bending of the lines observed experimentally can indeed be attributed to the wall
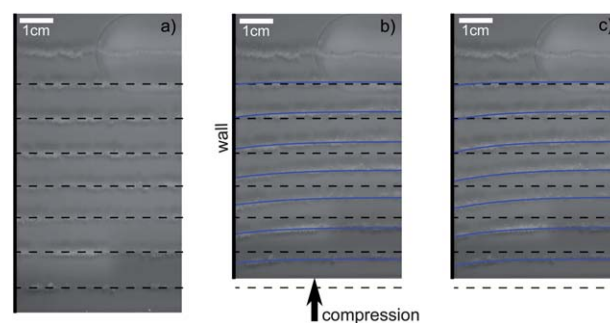
We have also seen that the width of the trough plays only a very limited role in determining the value of the collapse pressure that is measured. The study of the displacement of material lines placed in the layer prior to compression shows that friction with the wall does create a distortion of the strain field, but only in the vicinity of the walls (over a region around $w/4$ away from the wall). From this we conclude that the trough width should be expected to play little role in the measurement of surface pressures provided that the trough is wide enough and that the Wilhelmy plate is not in the region affected by wall friction. We see, therefore, that protein films do behave differently to particle rafts for which the trough width plays the dominant role.[10] From a modelling point of view, it seems that protein layers may indeed be treated as a thin elastic sheet despite the rigid character of individual hydrophobin molecules.[21] The size of the particles of the layer is presumably an important factor in determining when a system may behave like a granular raft, with the onset of granular behaviour likely to be in the colloidal regime.

The present study represents only a first step towards understanding this complicated system. In particular, we have been unable to explain the dependence of the surface pressure at collapse on either the distance between the barriers or the size of the Wilhelmy plate. Is this a result of the plate locally affecting the stress field within the layer (much as a crack or an inclusion can concentrate stresses[34]) or is it a result of the plate averaging the stress over a large area? Further investigation into this effect might use a non-invasive technique to measure the surface pressure, such as Surface Quasi-Elastic Light Scattering (SQELS).[35] At low pressures and elasticity the SQELS technique would be able to measure both the surface tension and the surface elasticity, whereas at higher pressures and elasticity it would be sensitive purely to the surface tension.[36] It is clearly very important to fully understand any limitations of using a Wilhelmy plate and Langmuir trough to measure surface pressures in systems with a finite shear elasticity.

Appendix 1: The compression rate does not affect the surface pressure at the onset of buckling

Films of polymers and proteins often display complex relaxation behaviour, and a relatively fast continuous compression in a Langmuir trough can shift the layer to a non-equilibrium state in which dilatational or shear stresses are not relaxed.[37] The elastic and shear moduli can be frequency dependent, and hence the stresses in the layer could depend on the strain rate (i.e. speed of compression).[8,38] In the experiments presented hitherto in this paper, hydrophobin layers have been compressed at a constant barrier speed corresponding to 30 cm² min⁻¹ at full trough width. This constant barrier speed means that a different strain rate is being applied depending on the trough area during the recording of the isotherm (a factor of 6 difference between maximum and minimum strain rates). There are systems for which this might be important: Zang et al.[39] for example have studied the viscoelastic properties of silica nanoparticle monolayers and have found a correlation between the surface pressure and the strain rate. Hilles et al.[40] found that even a very slow compression of poly-octadecylacrylate layer can lead to non-equilibrium states. One may wonder if the linear dependency of the surface pressure at

the onset of buckling on the barrier-to-sensor distance is not simply the result of the different strain rates applied. To check this, different isotherms of compression have been recorded at different linear speeds for a given spread amount of hydrophobin. Fig. 7a shows that the isotherms do not change systematically as the compression rate is changed. In particular, the surface pressure at buckling (obtained as described in Fig. 2 and shown in Fig. 7b) does not depend on the compression speed in the range that can be accessed by our instrument. While we cannot exclude the presence of dynamical relaxation in this layer, the data implies that any relaxation rates would be either much faster or much slower than the range of strain rates investigated in this study. This control experiment does not prove that the system is at equilibrium but shows that a different compression rate applied to the layer at different trough areas does not influence the surface pressure at the onset of buckling and cannot account for the surface pressure decay observed as the barrier-to-sensor distance increases.

Appendix 2: A model of frictional effects

In this Appendix, we present a mathematical model for the strain field within the layer. This model is used to calculate the
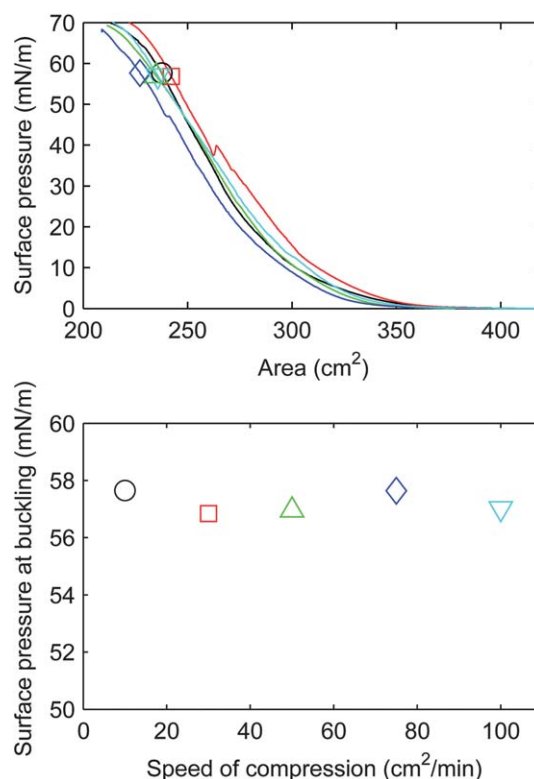

Fig. 7 The shape of the isotherm is not affected by the speed of compression in the whole experimental range. Panel (a) shows isotherms obatained at 10 cm² min⁻¹ (○), 30 cm² min⁻¹ (□), 50 cm² min⁻¹ (△), 75 cm² min⁻¹ (◇) and 100 cm² min⁻¹ (▽). Only for this control experiment, and for the purpose of removing the variability in the spread amount, the measurements were performed on the same layer which was first subjected to 3 compression/expansion cycles. The spread amount of hydrophobin was 85.2 μg. The surface pressure at the onset of buckling, shown in (b), is independent of the compression speed.

predictions for the position of the (initially straight) sulfur lines presented in Fig. 6. The model is based on the assumption that the layer behaves like a thin elastic plate with a Poisson ratio ν. The deformation field within the layer (u,v) then satisfies the equations of plane stress:[41]

$$2\frac{\partial^2 u}{\partial x^2} + (1-\nu)\frac{\partial^2 u}{\partial y^2} + (1+\nu)\frac{\partial^2 v}{\partial x \partial y} = 0 \quad (1)$$

$$2\frac{\partial^2 v}{\partial y^2} + (1-\nu)\frac{\partial^2 v}{\partial x^2} + (1+\nu)\frac{\partial^2 u}{\partial x \partial y} = 0. \quad (2)$$

The eqn (1)–(2) must be solved subject to appropriate boundary conditions. For simplicity, we take the origin of our Cartesian coordinate system to be at the centre of one of the walls, as shown in Fig.1. It is then only necessary to solve eqn (1)–(2) on the quarter-domain $0 \le x \le w/2$, $0 \le y \le d$ where the trough has width w and the distance between the barriers is $2d$.

Assuming that the imposed barrier displacement is Δv and that the layer is attached to the barrier we have boundary conditions along the barrier

$$u(x,d/2) = 0, \quad v(x,d/2) = \Delta v. \quad (3)$$

We also have the symmetry conditions

$$u(w/2,y) = 0, \left.\frac{\partial v}{\partial x}\right|_{(w/2,y)} = 0, \quad (4)$$

and

$$\left.\frac{\partial u}{\partial y}\right|_{(x,0)} = 0, \quad v(x,0) = 0. \quad (5)$$

Finally, we assume that along the wall the layer is on the point of sliding, and also that $u(0,y) = 0$. Mathematically, the sliding condition reads $\sigma_{xy} = \mu\sigma_{xx}$ where σ is the stress tensor and μ is a constant friction coefficient. In terms of displacements we have

$$2\mu\left(\frac{\partial u}{\partial x} + \nu\frac{\partial v}{\partial y}\right) - (1-\nu)\left[\frac{\partial u}{\partial y} + \frac{\partial v}{\partial x}\right] = 0 \quad (6)$$
$$\text{on } x = 0.$$

Eqn (1)–(2) were solved subject to the boundary conditions (3)–(6) using a finite difference method. The displacement is imposed incrementally (much as it is in the experiment itself) with the aspect ratio of the trough, $2d/w$, altered appropriately after each increment. The position of material lines placed at known locations within the undeformed layer are re-calculated at each step. We use a value for the Poisson ratio of $\nu = 0.5$ in the simulations reported here but simulations with other similar values of ν show no significant difference. It is not possible to measure ν directly because the layer fills the trough; it is not possible to measure the lateral expansion upon uniaxial compression. However, theoretical considerations for particle rafts[10,42,43] suggest a value $0.33 \lesssim \nu \lesssim 0.58$ motivating the value taken here.

Appendix 3: Analysis of deformed sulfur lines

Fig. 6 shows that the deformed shape of sulfur lines is reproduced by our model of an elastic sheet with a frictional wall boundary
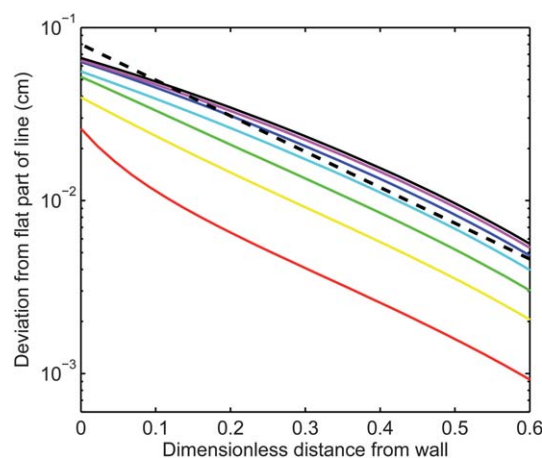

Fig. 8 The strain decays approximately exponentially away from the sides of the trough. The theoretically determined positions of the lines after deformation are shown here on semi-logarithmic axes. The dashed line shows the slope of $y \propto \exp(-x/0.21)$. In the theoretical calculations $\mu = 0.75$ and $\nu = 0.5$.

condition. From analysis of the simulation results, it seems that the lines can be approximated reasonably by a simple exponential function of the type $y = A\exp(-x/l) + y_c$, where x is the distance from the wall divided by half the trough width, see Fig. 8. For all of the results analysed, a value $l \approx 0.21$ provides a satisfactory fit.

To quantify the comparison between theoretical prediction of the deformation field and experimental observations we also performed a similar exponential fit to the experimental results. A Matlab routine was written to perform the fitting of each deformed line. The image is first sliced into frames that contain a single line each. The brightest pixel in each column corresponds to the most likely vertical position of the line. The coordinates of each line, obtained in this way, can then be fitted using the Matlab routine "fminsearch" which performs an unconstrained nonlinear optimization for a given fitting function. First, the optimization was performed using three free parameters A, l and y_c. It was observed that the value of l found in this way is approximately constant for each line with $l \approx 0.21$, consistent with the theoretical prediction. The fitting was then performed a second time, with the parameter l constrained to $l = 0.21$ and optimization performed only on the parameters A and y_c. Fig. 9 shows the exponential fitting for a trough width of 10 cm and a compression of 14%. These experiments (and fitting) were repeated for troughs of different widths. In each case the lines could be satisfactorily fitted with an exponential of decay length $0.21 \times w/2$, as predicted by the numerical simulations.

A second comparison between theory and experiment is the amplitude of the exponential decay, denoted by A. This parameter corresponds to the deviation from horizontal of each line and is shown in Fig. 10. We note that the theoretically predicted deviation and that observed experimentally agree well. Fig. 10 also shows that this deviation is maximum for lines midway between the barrier and the centre of the trough. The lines closest to the barrier will not be deformed much since the barrier is flat and the centre of the trough suffers no deformation (by
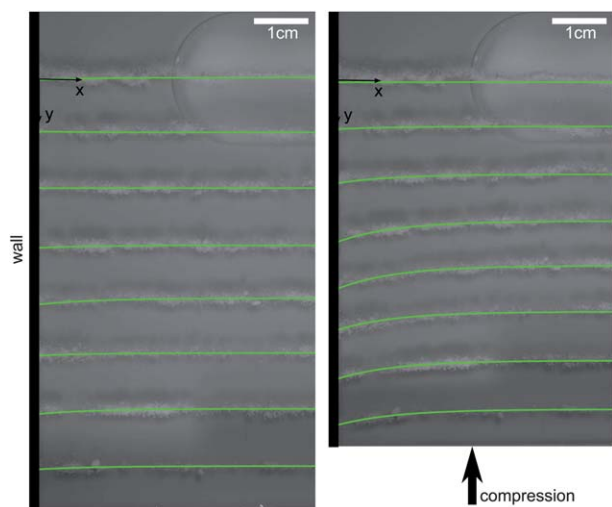
Fig. 9 The distortion field can be measured from image analysis. Sulfur lines sprinkled on an hydrophobin layer are imaged before (left) and after (right) a 14% compression. These images display a quarter of a trough, with the compressing barrier being at the bottom of the image and the trough wall on the left hand side. The sulfur powder displacement can be fitted by an exponential law $y = A\exp(-x/l) + y_c$, where the x - coordinate is normalised by the half width of the trough $w/2$ (solid lines).
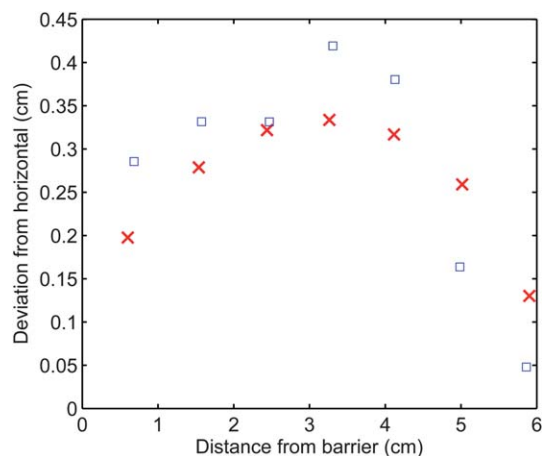

Fig. 10 There is good agreement between the experiments and the theoretical model for the strain in the layer, accounting for wall friction. The plot shows the theoretically predicted ($\times$) and experimentally observed ($\square$) values of the deviation from horizontal for the deformed lines shown in Fig. 9. In the theoretical calculations $\mu = 0.75$.

symmetry) so it is not surprising that the maximum deviation is observed midway between the two.

Acknowledgments

References

1 L. Wilhelmy, *Ann. Physik.*, 1863, **199**, 177–217.
2 G. Gaines, *Insoluble monolayers at liquid-gas interfaces*, Interscience Publishers, 1966, p. 46.
3 D. Möbius and R. Miller, *Proteins at liquid interfaces*, Elsevier, Amsterdam, 1998.
4 J. Benjamins and E. Lucassen-Reynders, in ref. 3, p.341.
5 A. Prins, M. Bos, F. Boerboom and H. van Kalsbeek, in ref. 3, p.221.
6 T. Kawanishi, T. Seimiya and T. Sasaki, *J. Colloid Interface Sci.*, 1970, **32**, 622.
7 P. B. Welzel, I. Weis and G. Schwarz, *Colloids Surf., A*, 1998, **144**, 229–234.
8 P. Cicuta and E. M. Terentjev, *Eur. Phys. J. E*, 2005, **16**, 147–158.
9 J. T. Petkov, T. D. Gurkov, B. E. Campbell and R. P. Borwankar, *Langmuir*, 2000, **16**, 3703–3711.
10 P. Cicuta and D. Vella, *Phys. Rev. Lett.*, 2009, **102**, 138302.
11 J. Peng and G. Barnes, *Langmuir*, 1990, **6**, 578–582.
12 M. Mate, J. H. Fendler, J. J. Ramsden, J. Szalma and Z. Horvolgyi, *Langmuir*, 1998, **14**, 6501–6504.
13 A. Prins and H. K. A. I. van Kalsbeek, *Colloids Surf., A*, 2001, **186**, 55–62.
14 J. Kumaki, *Macromolecules*, 1988, **21**, 749–755.
15 H. Yim, M. D. Foster, J. Engelking, H. Menzel and A. M. Ritcey, *Langmuir*, 2000, **16**, 9792–9796.
16 T. A. Witten, J. Wang, L. Pocivavsek and K. Y. C. Lee, *J. Chem. Phys.*, 2010, **132**, 046102.
17 C. Ybert, W. X. Lu, G. Moller and C. M. Knobler, *J. Phys. Chem. B*, 2002, **106**, 2004–2008.
18 J. J., S. T. Milner and P.P., *Europhys. Lett.*, 1989, **9**, 495–500.
19 C. Powell, N. Fenwick, F. Bresme and N. Quirke, *Colloids Surf., A*, 2002, **206**, 241–251.
20 K. D. Danov, P. A. Kralchevsky and S. D. Stoyanov, *Langmuir*, 2010, **26**, 143–155.
21 M. B. Linder, *Curr. Opin. Colloid Interface Sci.*, 2009, **14**, 356–363.
22 A. R. Cox, F. Cagnol, A. B. Russell and M. J. Izzard, *Langmuir*, 2007, **23**, 7995–8002.
23 T. B. J. Blijdenstein, P. W. N. de Groot and S. D. Stoyanov, *Soft Matter*, 2010, **6**, 1799–1808.
24 A. Paananen, E. Vuorimaa, M. Torkkeli, M. Penttil, M. Kauranen, O. Ikkala, H. Lemmetyinen, R. Serimaa and M. B. Linder, *Biochemistry*, 2003, **42**, 5253–5258.
25 M. J. Bailey, S. Askolin, N. Horhammer, M. Tenkanen, M. Linder, M. Penttila and T. Nakari-Setala, *Appl. Microbiol. Biotechnol.*, 2002, **58**, 721–727.
26 M. Linder, K. Selber, T. Nakari-Setala, M. Qiao, M.-R. Kula and M. Penttila, *Biomacromolecules*, 2001, **2**, 511–517.
27 B. R. Malcolm, *Langmuir*, 1995, **11**, 204–210.
28 V. Vontscharner and H. McConnell, *Biophys. J.*, 1981, **36**, 409–419.
29 M. M. Lipp, K. Y. Lee, A. Waring and J. A. Zasadzinski, *Biophys. J.*, 1997, **72**, 2783–2804.
30 T. Ferenczi and P. Cicuta, *J. Phys.: Condens. Matter*, 2005, **17**, S3445.
31 P. Cicuta and I. Hopkinson, *J. Chem. Phys.*, 2001, **114**, 8659.
32 G. S. Lapham, D. R. Dowling and W. W. Schultz, *Exp. Fluids*, 1999, **27**, 157–166.
33 K. Kisko, G. R. Szilvay, E. Vuorimaa, H. Lemmetyinen, M. B. Linder, M. Torkkeli and R. Serimaa, *Langmuir*, 2009, **25**, 1612–1619.
34 C. E. Inglis, *Royal Inst. of Naval Architects Trans.*, 1913, **55**, 219–230.
35 P. Cicuta and I. Hopkinson, *Colloids Surf., A*, 2004, **233**, 97.
36 D. M. A. Buzza, *Langmuir*, 2002, **18**, 8418.
37 D. Langevin, *Light Scattering by Liquid Surfaces and Complementary Techniques*, Marcel Dekker Inc., 1991.
38 P. Cicuta, *J. Colloid Interface Sci.*, 2007, **308**, 93–99.
39 D. Y. Zang, E. Rio, D. Langevin, B. Wei and B. P. Binks, *Eur. Phys. J. E*, 2010, **31**, 125–134.
40 H. Hilles, A. Maestro, F. Monroy, F. Ortega, R. G. Rubio and M. G. Velarde, *J. Chem. Phys.*, 2007, **126**, 124904.
41 L. Landau, E. Lifshitz, A. Kosevich, L. Pitaevskii, J. Sykes and W. Reid, *Theory of elasticity*, Butterworth-Heinemann, 1986.
42 D. Vella, P. Aussillous and L. Mahadevan, *Europhys. Lett.*, 2004, **68**, 212–218.
43 P. S. Clegg, *J. Phys.: Condens. Matter*, 2008, **20**, 113101.